Stabilizing Interfaces in High-Temperature NCM811-Li Batteries via Tuning Terminal Alkyl Chains of Ether Solvents

Zhijie Wang,[a]‡ Changsheng Chen,[a]‡ Danni Wang,[a] Ye Zhu,*[a] and Biao Zhang*[a]

[a] Dr. Z. Wang, C. Chen, D. Wang, Dr. Y. Zhu, Dr. B. Zhang
Department of Applied Physics & Research Institute for Smart Energy
The Hong Kong Polytechnic University
Hung Hom, Hong Kong 999077, People's Republic of China
E-mail: biao.ap.zhang@polyu.edu.hk; ye.ap.zhu@polyu.edu.hk
‡ These authors contributed equally.

Supporting information for this article is given via a link at the end of the document.

Abstract: Ether electrolytes are promising for lithium metal batteries. Despite the intensive research in recent years, most state-of-the-art ether electrolytes still cannot form reliable electrode-electrolyte interfaces in NCM811-Li batteries at diluted concentrations, especially in those operating at elevated temperatures. We report a simple but effective strategy to break this bottleneck and stabilize interfaces in high-temperature NCM811-Li batteries in ether electrolytes. We propose that by gradually extending the terminal groups of glycol diethers from methyl groups to *n*-butyl groups, the comprehensive stability of ether electrolytes is improved. An anion-dominated solvation structure is realized at a concentration of 1 M. Accordingly, the electrode-electrolyte interactions are suppressed, and a thinner, denser, and more inorganic-rich solid- /cathode-electrolyte interface is achieved. Additionally, the phase transition and structural degradation of NCM811 cathode are alleviated. Consequently, in the ethylene glycol dibutyl ether-based electrolyte, the Coulombic efficiency for Li-Cu cells working at 60 °C is boosted to 99.41% with a cycling life of over 200 cycles. The lifespan of high-temperature NCM811-Li cells is prolonged by more than 400% with a stable average Coulombic efficiency of 99.77% at quasi-practical conditions of 50 μm Li, lean electrolyte of 10 μL mAh^{-1}, and medium-high cathode loading of >2.2 mAh cm^{-2}.

Introduction

Metallic lithium (Li) has been regarded as the ultimate choice as an anode material for next-generation batteries because of its low density, high theoretical specific capacity, and lowest electrochemical potential.[1] When paired with nickel (Ni)-rich cathodes, such as $LiNi_{0.8}Co_{0.1}Mn_{0.1}O_2$ (NCM811), the energy density of lithium metal batteries (LMBs) is promising to approach 500 Wh kg^{-1},[2] which is two times higher than that of traditional Li-ion batteries (LIBs). However, the unstable electrode-electrolyte interfaces have been hindering the practical application of LMBs.[3] On the anode side, Li metal is thermodynamically unstable against electrolytes, and it will react with electrolytes to form a solid-electrolyte interphase (SEI).[4] The breakup and repair of SEI during repeated Li plating/stripping will continuously consume electrochemically active Li and electrolytes, thus shortening the lifespan of LMBs.[5] On the cathode side, the high valence Ni^{4+} of the charged NCM811 is reactive. It can easily oxidize the electrolytes, leading to the formation of a cathode-electrolyte interphase (CEI).[6] Moreover, due to the high energy barrier in the oxidation of Ni^{2+} to Ni^{3+} and the similar ionic radius of Ni^{2+} (0.69 Å) and Li^+ (0.76 Å), a cation mixing of Ni^{2+} and Li^+ also occurs on the cathode surface, triggering a transition of initial layered phase ($R\bar{3}m$) to rock-salt phase ($Fm\bar{3}m$).[7] The phase transition could further result in intragranular cracking, structural degradation, and capacity loss of NCM811 electrode.[8] Worse still, in real working conditions, continuous heat is generated so that LMBs are heated, which will unquestioningly boost the side reactions between electrodes and electrolytes and damage the stability of electrode-electrolyte interfaces.[6, 9]

To date, various interfacial engineering has been applied to tackle these challenges, such as developing artificial SEI layers for Li metal anode[10] and protecting NCM811 with inert layers[3c, 11]. Although the success, the coated layers would be destroyed by the volume changes of the electrodes during battery cycling, consequently limiting the long-term cyclability of LMBs. In addition, the coated layers also increase the volume/mass of the electrodes, sacrificing the overall energy density of LMBs. A more fundamental strategy is improving the stability of electrolyte against both Li anode and NCM811 cathode and constructing robust electrode-electrolyte interfaces, especially at high temperatures.[12] Ether-based electrolytes are promising because they are thermodynamically more stable against Li metal than ester-based counterparts.[13] Ethylene glycol dimethyl ether (EGDME), also known as dimethoxyethane (DME), is the most common ether solvent used in developing electrolytes for LMBs. However, its volatile nature (boiling point 84 °C) and low oxidation voltage (<4 V) make it hardly be used in NCM811-Li batteries, let alone those working at elevated temperatures. Increasing salt concentration in EGDME is useful to develop high-performance NCM811-Li batteries via extending the oxidation voltage of the electrolytes and forming anion-derived inorganic SEI/CEI,[14] but the electrolytes still suffer from drawbacks including high viscosity, low ionic conductivity, and high cost. Synthesizing EGDME-based fluorinated solvents,[15] such as fluorinated 1,4-dimethoxylbutane and fluorinated triethylene glycol, achieves significant progress in improving the performance of high-voltage and high-energy-density LMBs through extending electrochemical tolerance window and forming F-rich SEI/CEI. However, the complicated procedures, poor yield, and high cost bring difficulties to the practical application of these fluorinated solvents at this stage. Despite the most recent progress in manipulating the molecular structure of F-free ethers and developing anion-enriched solvation structure to build inorganic-rich SEI/CEI via decreasing the solvation ability of solvents,[16] the performance of the

electrolytes in high-temperature NCM811-Li batteries either is unsatisfactory or has rarely been studied.

Towards this end, we report that the electrode-electrolyte interfaces in high-temperature NCM811-Li batteries can be effectively stabilized via tuning terminal alkyl groups of ether solvents. We show that by simply extending the two terminal methyl groups in EGDME to ethyl groups (corresponding to ethylene glycol diethyl ether, EGDEE) and *n*-butyl groups (corresponding to ethylene glycol dibutyl ether, EGDBE) (**Figure 1a**), the comprehensive thermodynamic stability of electrolytes are improved accordingly (**Figure 1b**). Moreover, the proportion of the contact ion pairs (CIPs) and aggregates (AGGs) coordination in the electrolyte has been remarkably increased even at a diluted concentration of 1 M, which promotes the generation of anion-derived SEI/CEI species. Therefore, the side reaction of electrolyte against Li metal anode and NCM811 cathode has been suppressed, and a denser, thinner, and more inorganic-rich SEI/CEI has been achieved (**Figure 1c-e**). In addition, the rock-salt phase formation and intragranular cracks in NCM811 cathode have been alleviated. The average Coulombic efficiency (CE) of Li-Cu cells has been boosted to 99.41% in EGDBE-based electrolytes at 60 °C, with a prolonged cycling life of over 200 cycles. The lifespan of high-temperature NCM811-Li battery in EGDBE-based electrolytes has also been extended by 400% compared with those in EGDME-based electrolytes, even at harsh conditions.

Results and Discussion

The electrolytes are formulated by dissolving lithium bis(fluorosulfonyl)imide (LiFSI) into a mixture of EGDME/TTE, EGDEE/TTE, and EGDBE/TTE (all are 1/1 in volume) with a nominal concentration of 1 M, where TTE is 1,1,2,2-tetrafluoroethyl 2,2,3,3-tetrafluoropropyl ether. Note that the salt concentration in the glycol diethers is 2 M. The obtained electrolytes were respectively denoted as EGDME-E, EGDEE-E, and EGDBE-E. It should be noted that TTE is a commercially available solvent with a lower price than most fluorinated ethers, and its function in this work is to guarantee good kinetics and low viscosity in all electrolytes. As shown in **Figure S1**, with the addition of TTE co-solvent, the viscosity of EGDBE-E is reduced from 13.90/5.42 to 4.69/2.17 mPa s at room temperature (RT)/60 °C. Although this viscosity of EGDBE-E is slightly higher than that of EGDME-E and EGDEE-E (**Figure S1**), it is still of considerable value to achieve excellent cycling and rate performance. In addition, even though the EGDBE-E has a sacrifice in ionic conductivity compared with EGDME-E and EGDEE-E (**Figure S2**), because of the change of solvation structure (will be discussed later), it still delivers a high level of 4.01/5.66 mS cm^{-1} at RT/60 °C, which is comparable with or higher than state-of-the-art electrolytes for LMBs.

The widely used EGDME has a low boiling/flash point of 84/−2 °C. With the extension of terminal alkyl groups, the alkoxy groups in EGDME are changed to ethoxy groups in EGDEE and *n*-butoxy groups in EGDBE, and the boiling/flash points are increased to 121/35 and 203.3/85 °C, respectively (**Table S1**). Thermogravimetric analysis (TGA) results in **Figure S3** show that most weight loss occurs below 100 °C in both EGDME-E and EGDEE-E, but the weight of EGDBE-E remains 55.1% at 100 °C. Note that the weight loss of EGDBE-E below 100 °C is mainly attributed to the evaporation of TTE, whose boiling point is only 92 °C. After being heated to 180 °C, the weight remaining is 17.6%, 21.6%, and 32.3% for EGDME-E, EGDEE-E, and EGDBE-E, respectively. These data prove that with the extension of terminal alkyl chains in ethers, the thermal evaporation of the electrolytes has drastically suppressed.

The thermodynamic stability of these electrolytes was studied with the density functional theory (DFT) method. The structure of the electrolytes was first simulated with the ab-initio molecule dynamics (AIMD) method (**Figure S4a-c**), and then their projected density of states (PDOS) was computed. As displayed in **Figure S4d-f**, the lowest unoccupied molecular orbital (LUMO) of EGDME-E is 2.95 eV, whilst that of EGDEE is increased to 3.05 eV. Surprisingly, the LUMO of EGDBE-E is remarkably promoted to 3.48 eV. This theoretically demonstrates that the reduction stability of electrolytes against Li metal has been dramatically improved.[17] In addition, the H-transfer energy of EGDME, EGDEE, and EGDBE molecules on de-lithiated NCM811 is calculated to be −1.285, −1.069, and −0.946 eV (**Figure S5**), respectively, reflecting an increased trend in the oxidation tolerance of these electrolytes against de-lithiated cathode.[18] The computation results for the bond dissociation energy in **Figure S6** show that the C-O and C-C bonds near ethereal oxygen atoms are labile, which agrees with the published results.[19] In contrast, the C-C bonds in the terminal alkyl chains are much more stable, where the farther from the ethereal oxygen atoms, the higher the dissociation energy. Thus, the proportion of stable parts in the whole ether chains gradually increases in EGDEE and EGDBE, compared with that in EGDME. Based on these results, it can be concluded that the comprehensive thermodynamic stability of EGDME-E, EGDEE-E, and EGDBE-E progressively increases, as illustrated in **Figure 1b**.

The chemical environment around Li^+ in these electrolytes was studied with nuclear magnetic resonance (NMR) spectroscopy. As shown in **Figure 1f**, from EGDME-E to EGDBE-E, the ^7Li NMR spectra have a slight downfield shift. This demonstrates the electron density around Li^+ is reduced, which can be attributed to the decreased solvation of ether solvents and the increased solvation of anions.[20] Raman spectra further verify this. As shown in **Figure S7**, the blue shift of the C-O-C stretching peak, caused by Li^+ coordination, is 27.4 cm^{-1} in EGDME-E, whilst those in EGDEE-E and EGDBE-E reduce to 16.1 and 2.9 cm^{-1}, respectively. Similarly, the blue shift of C-H stretching peak of alkyl groups in ethers is 17.1, 13.3, and 8.1 cm^{-1} in EGDME-E, EGDEE-E, and EGDBE-E, respectively (**Figure S8**), which also shows a downtrend. More importantly, the coordination status of FSI^- anion is quite different in these three electrolytes. The Raman spectra in **Figure S9** show that the proportion of solvent-separated-ion-pair (SSIP) coordination becomes smaller, but that of aggregate (AGG) coordination becomes larger when extending the terminal alkyl chains. The majority of FSI^- anions in EGDME-E exist as solvent-separated-ion-pair (SSIP). In contrast, those in EGDEE-E and EGDBE-E are contact-ion-pair (CIP) and aggregate (AGG) coordination, respectively. Surprisingly, the total proportion of CIP and AGG in EGDBE-E reaches 66%, which would help to generate an anion-derived SEI/CEI. The difference in the solvation structure of these electrolytes is illustrated accordingly in **Figure 1g-i**.

The improved electrolyte stability and the optimized solvation structure benefit the stabilization of the electrode-electrolyte interfaces, thus improving the lifespan of MCM811-Li batteries working at elevated temperatures. Detailed experimental evidence will be discussed in later sections.

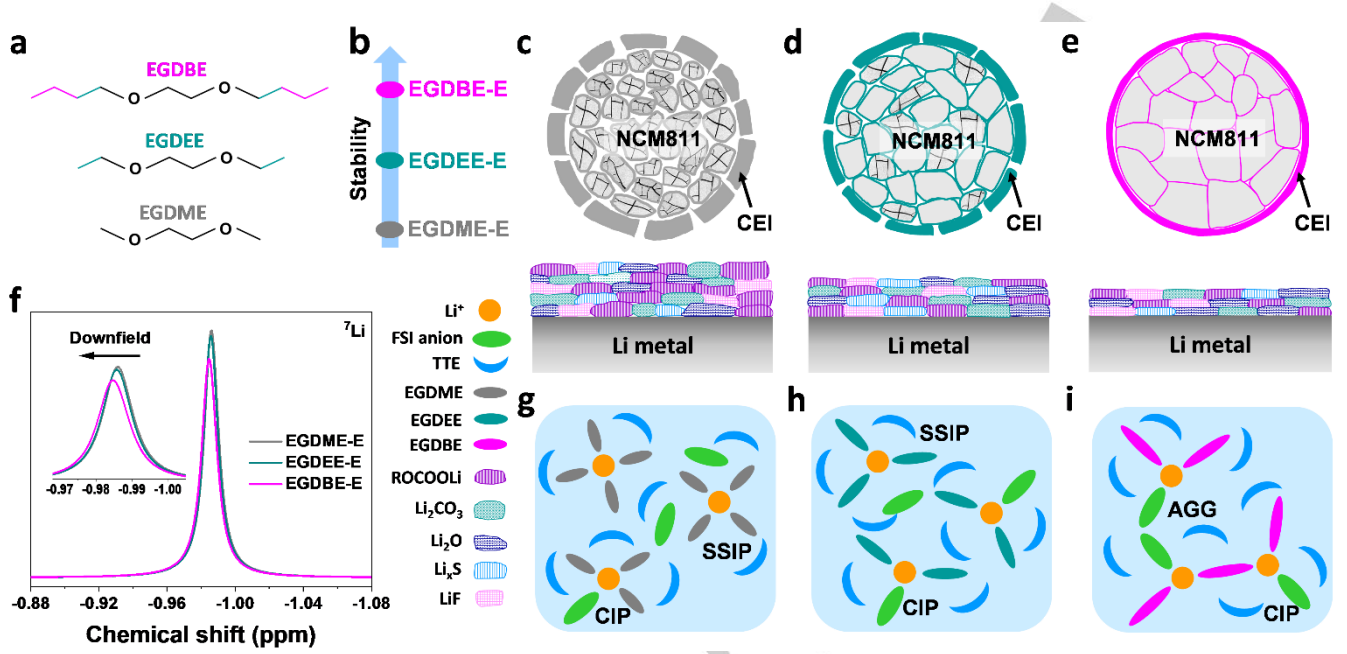

Figure 1. Design of the electrolytes and the effects on stabilizing electrode-electrolyte interfaces. (a) Molecular structure of EGDME, EGDEE, an EGDBE. (b) Illustration of the comprehensive stability comparison of EGDME-E, EGDEE-E, and EGDBE-E. Illustration of the effects of EGDME-E (c), EGDEE-E (d), and EGDBE-E (e) on the interfacial property of NCM811 cathode and Li metal anode. (f) ^{7}Li NMR spectra of the electrolytes. Schematic illustration of the solvation structure of EGDME-E (g), EGDEE-E (h), and EGDBE-E (i).

The morphology of Li plating on Cu foil is granular without tubular-like structure at both room temperature (**Figure S10**) and 60 °C (**Figure S11** and **Figure 2a-c**), demonstrating the excellent ability of ether-based electrolytes in suppressing Li dendrite growth. Though this, it still can be found that the plated Li becomes denser and flatter with the extension of terminal alkyl chains in ether solvents. Atomic force microscopy (AFM) 3D topographic images further reveal that the average surface roughness (Ra) of Li deposited in EGDME-E, EGDEE-E, and EGDBE-E at 60 °C are 518, 253, and 90 nm, respectively (**Figure S12**).

Li-Cu cells were tested to quantitatively measure the reversibility of Li plating/stripping efficiency. As shown in **Figure 2d**, following a short activation, the CE in all electrolytes reaches a level of >98.5%, and the average CE is 98.71%, 98.89%, and 99.13%, in the EGDME-E, EGDEE-E, and EGDBE-E, respectively. The CE in EGDME-E and EGDEE-E fluctuates and gradually drops after 100 cycles, accompanied by increased voltage polarization or unstable charging curves (**Figure 2g** and **Figure S13**). In striking contrast, the CE for the cell in EGDBE-E is stable for more than 250 cycles. When further increasing the concentration of LiFSI salt in EGDBE-E to 1.75 and 2.5 M (near saturated) (3.5 and 5 M in EGDBE solvent, respectively), the voltage polarization of Li-Cu cells greatly increases by more than 3 and 4 times, respectively, whilst the lifespan of Li-Cu cells decreases to only ~120 cycles (**Figure S14**). This proves that developing high concentration electrolyte based on EGDBE-E is not promising, due probably to the surged viscosity.

Li-Cu cells working at 60 °C were tested to evaluate the high-temperature performance of the electrolytes. As shown in **Figure S15**, the voltage polarization in all electrolytes decreases because of the improved reaction kinetics at high temperatures.[21] The CE in EGDME-E and EGDEE-E fluctuates and declines in succession after 70 and 80 cycles, but that in EGDBE-E is stable for over 200 cycles (**Figure 2e**,**h** and **Figure S15**). It is worth noting that the average CE of Li-Cu cell in EGDBE-E reaches 99.41% at 60 °C. To the best of our knowledge, in previously reported electrolytes, the CE for high-temperature (≤60°C) Li-Cu cells is lower than 99.3% at a current density of ≤1 mAh cm^{-2} (**Table S3**). Even at a high current density of 3 and 5 mA cm^{-2}, Li-Cu cells deliver a high average CE of 99.22% and 99.01% in EGDBE-E (**Figure S16**), with a lifespan of >125 and >100 cycles, respectively. The high-temperature CE achieved in EGDBE-E is among the highest records reported so far.

To exclude the influence of TTE co-solvent, Li-Cu cells in the electrolyte without TTE were tested at 60 °C. As shown in **Figure S17**, the initial CE (ICE) of Li-Cu cells in electrolytes 2 M LiFSI in EGDME (EGDME-E without TTE), 2 M LiFSI in EGDEE (EGDEE-E without TTE), and 2 M LiFSI in EGDBE (EGDBE-E without TTE), is 92.74%, 95.05%, and 95.56%, respectively. The CE in 2 M LiFSI in EGDME gradually drops with cycling, with a low average value of 95.99%. The CE in 2 M LiFSI in EGDEE and 2 M LiFSI in EGDBE is close in the initial 100 cycles. However, the former one drops and vibrates after 115 cycles, but the latter one is stable for more than 140 cycles. The average CE after activation in electrolyte 2 M LiFSI in EGDBE is 99.22%, which is only slightly lower than that in EGDBE-E (with TTE). These results demonstrate that tuning terminal alkyl groups plays the dominant role in boosting the CE of Li-Cu cells, while the addition of TTE co-solvent contributes to the kinetics by decreasing the viscosity.

Li-Li symmetric cells with thin Li foils (50 μm) were also tested at 60°C to validate the reversibility of Li anode in these electrolytes. The cells are cycled at a current density of 1 mA cm^{-2} with an area capacity of 1 mAh cm^{-2}, corresponding to a depth of discharging (DOD) of 10%. As shown in **Figure 2f**, the Li-Li cells in EGDME-E undergo a gradual increase in voltage polarization starting from ~1150 h due to the depletion of electrochemically active Li. In strong contrast, the cells in EGDEE-E show a stable discharging-charging profile for ~1380 h, which is further boosted to over 1700 h in EGDBE-E. Particularly, a low voltage polarization of merely ~45 mV is observed in EGDBE-E (**Figure 2i** and **S18**). When the current density increased to 3 and 5 mA cm^{-2}, the Li||Li cells still deliver a lifespan of more than 530 and 275 h in EGDBE-E (**Figure S19**), respectively.

In addition to the above-discussed high-temperature performance, the Li-Cu cells with EGDBE-E at low temperatures were also explored. As shown in **Figure S20**, it shows a decent average CE of 98.5% at 0 °C. The value decreases to 96.5% with remarkably increased voltage polarization at −25 °C, reducing the potential for applying at super-low temperature.

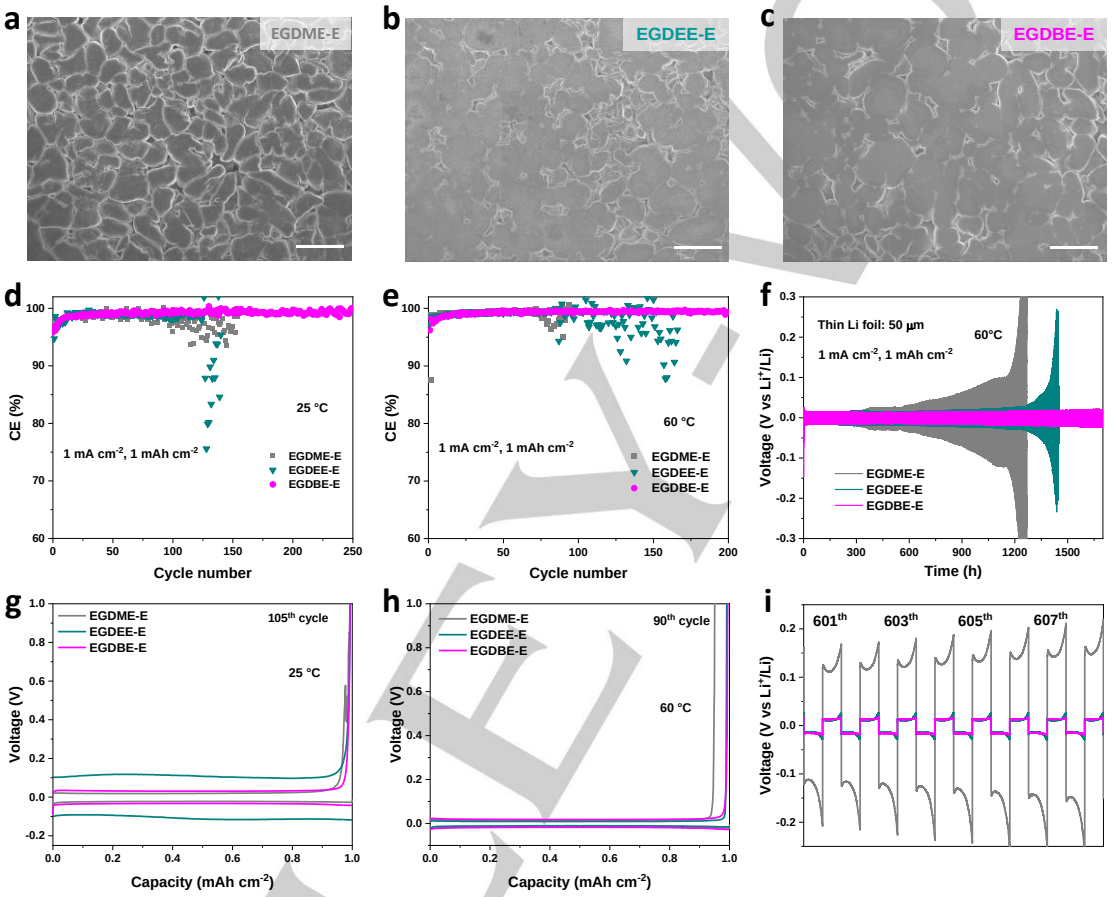

Figure 2. Reversibility of Li metal anode. SEM images of Li plated on Cu foil in EGDME-E (a), EGDEE-E (b), and EGDBE-E (c). The current density is 0.5 mA cm^{-2} and the capacity is 5 mAh cm^{-2}. Scale bars: 20 μm. CE for Li plating/stripping in Li-Cu cells in these electrolytes at 25 (d) and 60 ℃ (e), and the corresponding voltage profiles at 25 (g) and 60 ℃ (h). Voltage profiles of Li||Li symmetric cells cycled in these electrolytes at 60 ℃ (f) and an enlarged region (i).

The morphology and interfacial properties of Li metal anodes cycled Li-Cu cells at 60 °C were further examined. As shown in **Figure S21**, the surface of Li cycled in EGDEE-E (Li@EGDEE-E) is loose and crushed, and the situation in Li cycled in EGDME-E (Li@EGDME-E) is much worse. In sharp contrast, the Li cycled in EGDBE-E (Li@EGDBE-E) is much flatter, and its surface is full of granular Li. Cross-sectional SEM images in **Figure S22** also reveal that the surface of Li@EGDME-E and Li@EGDEE-E is covered by a cracked "dead" Li layer generated by non-uniform Li stripping and following SEI isolation,[22] but that of Li@EGDBE-E becomes much compacter. The flatter and compactor surface of Li@EGDBE-E is also quantificationally verified by AFM 3D topographic mapping results. As shown in **Figure 3a** and **Figure S23**, the Ra for the surface of Li@EGDBE-E is 46 nm, much lower than those of Li@EGDME-E (294 nm) and Li@EGDEE-E (123 nm).

Time-of-flight secondary ion mass spectrometry (TOF-SIMS) and X-ray photoelectron spectroscopy (XPS) tests were further performed to study the surface chemistry of cycled Li metal anodes. It can be seen from the TOF-SIMS depth profiles in **Figure S24**, in all cycled Li electrodes, the intensity for ^{6}Li and ^{7}Li secondary ions increases with sputtering, indicating the signal of metallic Li becomes stronger along the depth direction. Importantly, the intensity of these two ions increases in the order of Li@EGDME-E, Li-EGDEE-E, and Li@EGDBE-E. In addition, as shown in the normalized depth profiles and the 3D rendering images in **Figure 3b** and **Figure S25**, the intensity of these two ions reaches a maximum after sputtering for 130 s in Li@EGDBE-

E, but those time in Li@EGDME and Li@EGDEE-E are 360 and 210 s, respectively. A same trend can be found in the Li 1s XPS depth profile. As shown in **Figure 3c**, in each sputtering, the Li^0 signal, which refers to metallic Li, becomes stronger in the order of Li@EGDME-E, Li@EGDEE-E, and Li@EGDBE-E. After sputtering for 300 s, the Li^0 peak of Li@EGDBE-E is obviously higher than those former two samples. These results demonstrates that the vanishing of SEI and detection of metallic Li underneath SEI become earlier with the extension of the terminal alkyl chains of the solvents, confirming the thickness of SEI formed on Li is reduced accordingly. This can be attributed to the supressed side reaction between electrolyte and Li, which originates from the improved thermodynamic stability of the electrolyte.

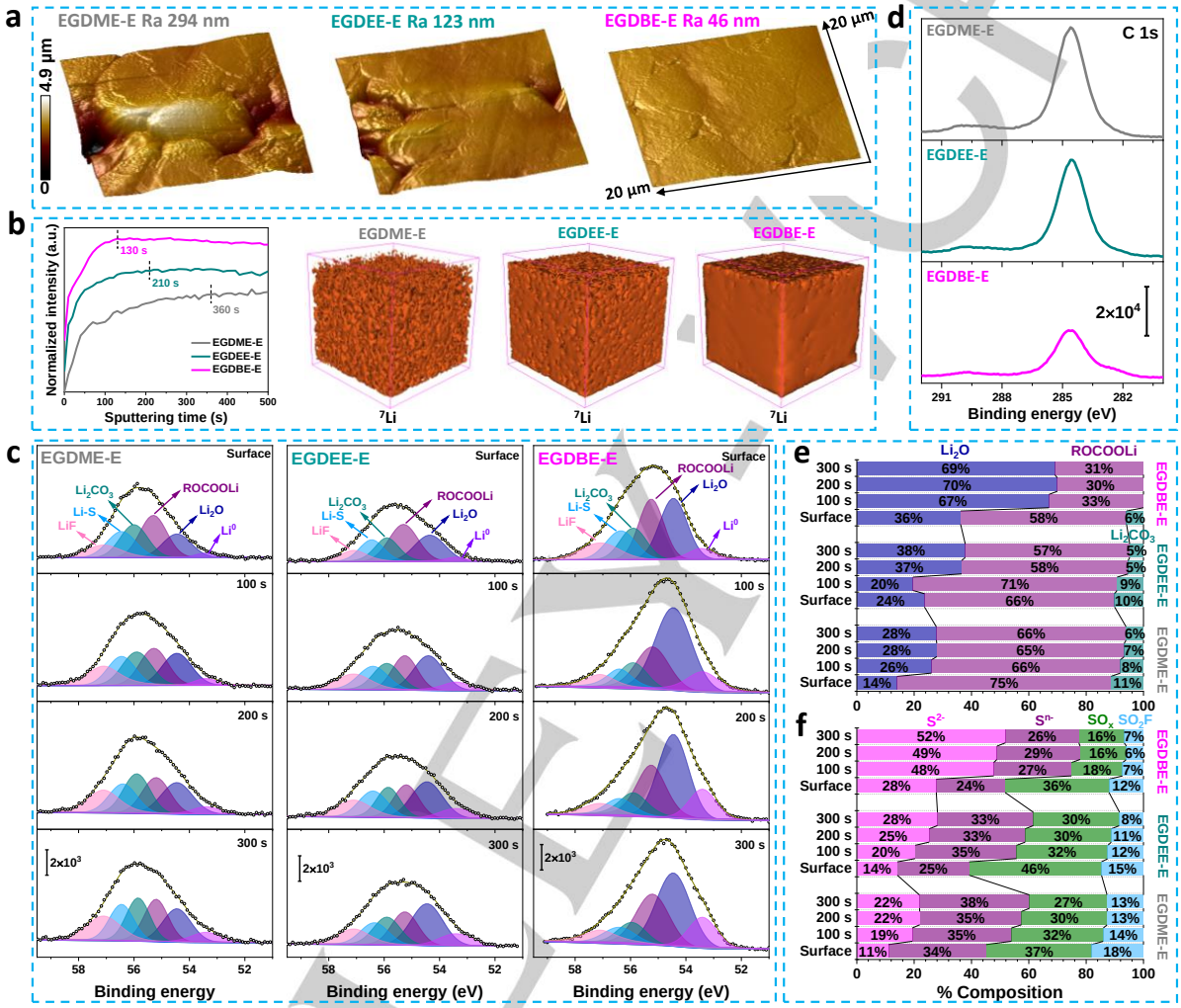

Figure 3. Surface property of Li metal anodes cycled in Li-Cu cells for 50 cycles at 60 ℃. (a) The AFM 3D topography images of Li electrodes cycled at 60 °C in EGDME-E, EGDEE-E, and EGDBE-E. TOF-SIMS depth profiles for ^7Li secondary ion and the corresponding 3D rendering images (b), C 1s XPS spectra (c), and Li 1s XPS depth profiles (d) of Li electrodes cycled at 60 °C in EGDME-E, EGDEE-E, and EGDBE-E. The roter size in (b) is 400 μm x 400 μm. Analysis for O-containing species based on O 1s XPS spectra (e) and S-containing species based on S 2p XPS spectra (f).

In the surface C 1s XPS spectra (**Figure 3c**) and the C 1s depth profiles (**Figure S26**), the intensity of the C-C, C-O, and poly(CO_3) peaks reduces in order of Li@EGDME-E, Li@EGDEE-E, and Li@GDBE-E, demonstrating that the decomposition of C-containing components, the solvents, on Li metal anode decreases accordingly. A similar phenomenon can be observed in Li 1s XPS depth profiles. As shown in **Figure 3b**, in Li@EGDME-E, ROCOOLi and Li_2CO_3, the decomposition products of glycol ethers, dominate the Li 1s spectra from surface to sputtering for 300 s. In Li@EGDEE-E, the peak intensity of ROCOOLi and Li_2CO_3 decreases whilst that of Li_2O, which comes from the decomposition of FSI^- anion, increases. After a sputtering of 300 s, the Li_2O peak is slightly stronger than ROCOOLi and Li_2CO_3 peaks. In Li@EGDBE-E, however, the intensity of the Li_2O peak becomes remarkably higher than those of ROCOOLi and Li_2CO_3 peaks after sputtering for only 100 s, and then it dominates the spectra and preserves with continuous sputtering. O 1s depth profiles in **Figure S27** also show similar results. The analysis based on O 1s depth profiles in **Figure 3e** reveals that after sputtering for 300 s, the proportion of Li_2O in Li@EGDME-E, Li@EGDEE-E, and Li@GDBE-E is 28%, 38%, and 69%, respectively. Those of ROCOOLi or Li_2CO_3 have a reverse trend, which are 72%, 62%, and 31%, respectively. Furthermore, the F 1s depth profiles in **Figure S28** indicate that

the content of LiF in the SEI of Li metal anodes cycled in these three electrolytes decreases accordingly, which agrees well with that in Li 1s depth profiles. The LiF mainly comes from the decomposition of TTE on the Li metal anode, which does not have solvation ability but could react with Li metal.[23]

To further explore the reason for the distinct SEIs in the three electrolytes, S 2p and N 1s XPS depth profiles were analysed. SO_2F group of FSI^- anion has been partially reduced on all cycled Li (**Figure S29**). As the sputtering depth increases, more SO_2F is reduced. The most significant difference in these samples is the reduction degree of SO_2F. As shown in **Figure 3f**, the total proportion of S^{2-} and S^{n-} in S-containing species increases in the order of Li@EGDME-E, Li@EGDME-E, and Li@EGDME-E. After sputtering for 300 s, these values in three samples are 60%, 61%, and 78%, respectively. Particularly, half (52%) of S-containing species is S^{2-} in Li@EGDBE-E, while those in Li@EGDEE-E and Li@EGDME-E are only 28% and 22%, respectively. The S^{2-} is assigned to Li_2S, which has a high ionic conductivity of ~10^{-5} S cm^{-1}.[24] The TOF-SIMS depth profiles and the corresponding 3D rendering images also show that the intensity of LiS secondary ion increase in the order of Li@EGDME-E, Li-EGDEE-E, and Li@EGDBE-E (**Figure S30**), providing additional evidence that the concentration of Li_2S or Li_nS in SEI is boosted in these Li electrodes accordingly. The N 1s depth profiles in **Figure S31** also validate that the reduction of the N-S group of FSI^- is the most on Li@EGDBE-E and the least on Li@EGDME-E. Therefore, it can be confirmed that the reduction of FSI^- anion on the surface of the Li metal anode has been promoted. More inorganic-rich SEI is generated along the extension of terminal alkyl chains in ethers. This can be attributed to the increased CIP and AGG coordinates in the electrolytes. The FSI^- anion-derived inorganic species, including Li_2O, Li_2S, and Li_nS, etc., can facilitate fast Li^+ diffusion but block electron tunneling through SEI and thus suppress Li dendrite growth and reduce the thickness of SEI.[25]

The electrochemical performance of NCM811-Li batteries in these electrolytes was initially evaluated at mild conditions, i.e., moderate NCM811 mass loading (5 mg cm^{-2}), exceeded Li (500 µm), and flooded electrolyte (50 µL). As shown in the tests at 0.5 C and 25 °C in **Figure 4a**, the capacity of NCM811-Li cell in EGDME-E electrolyte gradually decreases with cycling and occurs a sudden decline after 135 cycles. The cell in EGDEE-E could work stably for 170 cycles, followed by a rapid capacity drop. The cell with EGDBE-E, however, delivers much better cycling stability, with a capacity retention of 91.8% after 300 cycles (based on the first discharging capacity after activation, similarly hereinafter). Notably, the corresponding CE in EGDBE-E is obviously higher and more stable than those in EGDEE-E and EGDME-E, especially in the initial 40 cycles (**Figure S32**). The developed EGDBE-E is versatile and also effective for LCO-Li and NCA-Li batteries, where LCO and NCA refer to $LiCoO_2$ and $LiNi_{0.9}Mn_{0.08}Al_{0.02}O_2$ cathode, respectively (**Figure S33**). Besides, NCM811-graphite battery can also work stably in EGDBE-E, with a high average CE of >99.85% after activation (**Figure S34**). This work focuses on the NCM811-Li battery to demonstrate its application in high-temperature and high-energy-density batteries.

The high-temperature performance of NCM811-Li batteries was studied at 60 °C. Firstly, to investigate the effects of TTE co-solvent, the cycling performance of the batteries in electrolytes without TTE co-solvent were tested. As shown in **Figure S35**, the lifespan of the batteries in the electrolytes 2 M LiFSI in EGDME (EGDME-E without TTE), 2 M LiFSI in EGDEE (EGDEE-E without TTE), and 2 M LiFSI in EGDBE (EGDBE-E without TTE) is 38, 55, and more than 100 cycles (based on capacity retention of 80%), respectively. The corresponding CE also becomes obviously higher and more stable accordingly. In addition, through characterizing the NCM811 cathode after 50 cycles, it can be found that the thickness of CEI and phase transition layer on the cathode has been effectively reduced (**Figure S36**), confirming the side reaction between NCM 811 and electrolytes has been suppressed. The results endorse that extending the terminal alkyl groups in ether solvents can effectively improve the interfacial properties and electrochemical performance of NCM811-Li batteries. The addition of TTE further improves the lifespan of NCM811-Li batteries, mainly because of the decreased viscosity of the electrolytes. As shown in **Figure 4b**, the lifespan of NCM811-Li batteries in EGDME-E and EGDEE-E is improved 67 and 85 cycles, respectively. In particular, the battery in EGDBE-E delivers a long lifespan of 200 cycles. Its CE is also higher than those of the former two batteries, especially in the initial 30 cycles (**Figure S37**).

The rate performance of NCM811-Li batteries in the electrolytes was also tested at 60 °C. As shown in **Figure S38**, even at a high current density of 4 C, the capacity retention of the batteries is 67.7%, 67.6%, and 66.7% in EGDME-E, EGDEE-E, and EGDBE-E, respectively, compared with that at 0.5 C. Thus, it can be concluded that, although the ionic conductivity of the electrolytes decreases with the extension of terminal alkyl chains of ether solvents, there is no obvious sacrifice in the rate performance of NCM811-Li batteries. This should be attributed to the reduced interfacial impedance (**Figure S39**) arising from the improved electrode-electrolyte interfaces (will be discussed later).

To evaluate the performance of these electrolytes in quasi-practical conditions, high-temperature NCM811-Li batteries with medium-high cathode mass loading of 10 mg cm^{-2} (>2.2 mAh cm^{-2}), thin Li (50 µm), and lean electrolytes (10 µL mAh^{-1}), were further tested, in which the negative/positive (n/p) capacity ratio is ~4. The capacities of batteries in EGDME-E and EGDEE-E gradually fade, and their CE fluctuates and eventually fails after around 25 and 62 cycles (**Figure 4c**), respectively, because of the overcharging of electrolytes (**Figure 4d** and **Figure S40**). Surprisingly, the battery in EGDBE-E could deliver a lifespan of over 140 cycles (based on capacity retention of 80%), which is 3.7 and 1.1 times higher than those in EGDME-E and EGDEE-E, respectively. In addition, the battery in EGDBE-E delivers stable CE, with a high average of 99.77%, without any overcharging. In previously reported electrolytes, the lifespan of practical LMBs with NCM or NCA cathodes is limited to ~100 cycles at ~60°C, with a poor average CE of <99.5%. As compared in **Table S4**, the performance of high-temperature NCM811-Li batteries in EGDBE-E is much superior to those in most state-of-the-art electrolytes. To demonstrate the potential of practical application of EGDBE-E, a 0.5 Ah (500mAh) NCM811-Li pouch cell was fabricated and tested (**Figure 4e**), where the mass loading of NCM811 is ~10 mg cm^{-2}, the thickness of Li anode is 50 µm, and the electrolyte amount is ~5 µL mAh^{-1} (lean electrolyte). As shown in **Figure 4f**, the pouch cell works stably for more than 80 cycles at an impulse temperature variation of 25 and 60°C, with a high CE of >99.7% and a capacity retention of 91%.

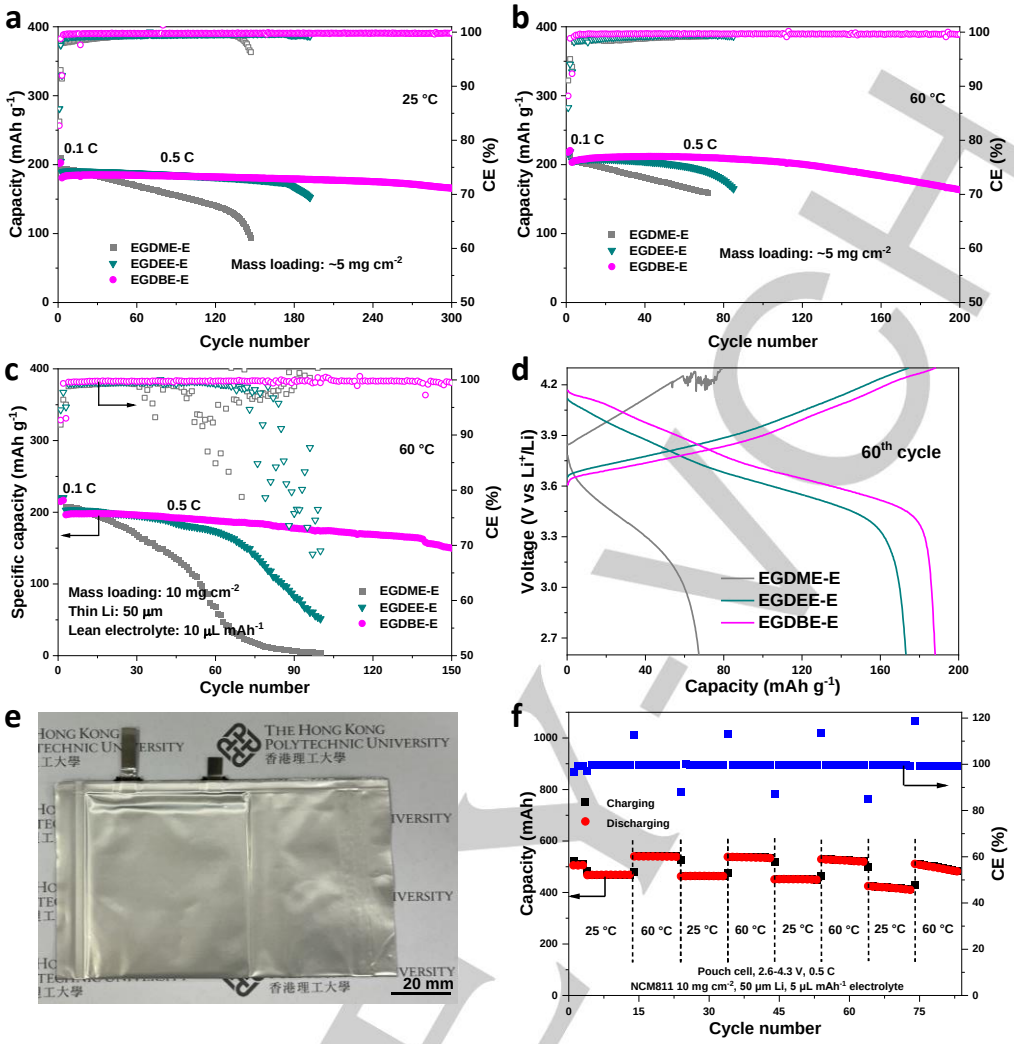

Figure 4. Electrochemical performance of NCM811-Li cells. NCM811-Li cell test in the three electrolytes at mild conditions at 25 (a) and 60 ℃ (b). NCM811-Li cell test in the three electrolytes at practical conditions at 60 ℃ (c), and the corresponding discharging-charging curves at the 60th cycle (d). Digital photo (e) and cycling performance (f) of a 0.5 Ah pouch cell with EGDBE-E. The cell was activated at 0.2 C for 3 cycles and cycled at 0.5 C.

To explore the mechanism of the improved performance of high-temperature NCM811-Li batteries, the CEI of cycled NCM811 at 60 °C is characterized with XPS. As shown in the O 1s spectra in **Figure 5a**, the intensity of M-O peaks (lattice oxygen) slightly increases in the order of NCM811 cycled in EGDME-E, EGDEE-E, and in EGDBE-E (denoted as NCM@EGDME-E, NCM@EGDEE-E, and NCM@EGDBE-E, respectively). This indicates the thickness of CEI layers formed on these cathodes reduces accordingly. At the same time, the intensity of C-O and CO_3 peaks decreases, confirming that the oxidation decomposition of the solvents has been suppressed. Furthermore, the increases in the intensity of S-O (**Figure 5a**) and Li-O-F (**Figure 5b**) peaks suggest that the decomposition of FSI^- anions on the surface of NCM811 is promoted, which could help to form more an inorganic-rich CEI. Interestingly, the intensity of C-F peaks decreases whilst that of LiF peaks increases. The C-F containing species should be generated from the decomposition of TTE or be assigned to PVDF. Given that the NCM811 electrodes are prepared at identical conditions, the contribution of PVDF to the C-F signal should have no significant difference in these three samples. Thus, it can be inferred that the decomposition of TTE on NCM811 is alleviated in EGDBE-E. Further, the increase in the intensity of the LiF peak should be attributed to the decomposition of FSI^- anions. Benefiting from these improvements in CEI, the dissolution of the Mn element of NCM811 is mitigated with the extension of the solvent terminal alkyl chains, as evidenced by the decreased intensity of Mn 2p spectra in **Figure 5c**, which also helps to reduce the capacity loss of NCM811-Li battery upon cycling.[26]

The structure of cycled NCM811 cathode was examined to further study the cathode-electrolyte interactions. First, the NCM811 electrodes cycled at 60 °C for 100 cycles were studied with a focused ion beam (FIB)-SEM. There is no significant morphological difference in the secondary NCM811 particles cycled in the three electrolytes (**Figure S41**). However, after FIB cutting, obvious cracks among the primary particles can be observed in NCM@EGDME-E (**Figure 5d** and **Figure S42a**), which could be attributed to the side reaction between the cathode and electrolyte. These cracks become much fewer in NCM@EGDEE-E (**Figure 5d** and **Figure S42b**), and finally

disappear in NCM811@EGDBE-E (**Figure 5d** and **Figure S42c**). The compacter and denser structure means that the NCM@EGDBE-E has higher integrity upon battery cycling, contributing to the improved lifespan of the NCM811-Li battery at high temperatures.

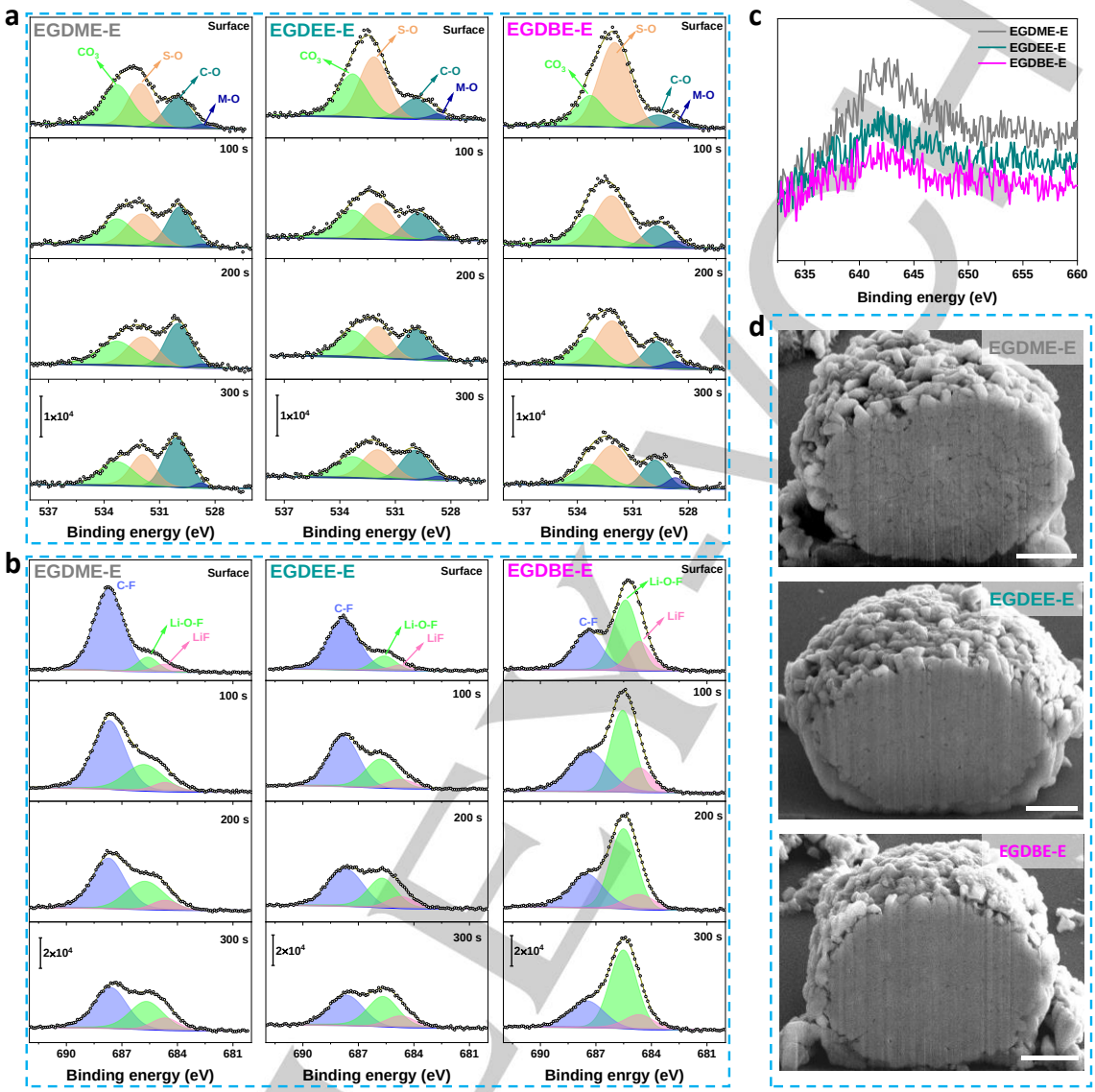

Figure 5. Surface chemistry and structure of NCM811 cathodes cycled in three electrolytes for 100 cycles at 60 ℃. F 1s (a) and O 1s (b) XPS depth profiles of cycled NCM811 cathodes. (c) Mn 2p XPS spectra of cycled NCM811 cathodes. Cross-sectional FIB-SEM images of NCM811 cycled in EGDME-E (d), EGDEE-E (e), and EGDBE-E (f). Scale bars: 2 μm.

Then, the primary particles of the cycled NCM811 cathodes were studied with annular bright-field scanning (ABF) and high-angle annular dark-field (HAADF) transmission electron microscopy (STEM), while the lamina samples were prepared by FIB-SEM. It can be found that there are many fine intragranular cracks throughout the NCM811@EGDME-E (**Figure 6a** and **Figure S43a**), and an obvious cation mixing layer (rock-salt phase) of 1-2 nm covers the inner surface of the cracks (**Figure 6d** and **Figure S44a**). Besides, defective regions, which may come from the corrosion of electrolytes, can be found near the cracks (**Figure 6d** and **Figure S45**). In NCM@EGDEE-E, although intragranular cracks still can be found, the number is much fewer (**Figure 6b** and **Figure S43b**). Similar rock-salt layers were also formed on the cracks' inner surface, but no obvious defective regions can be observed (**Figure 6e** and **Figure S44c**). In sharp contrast, the NCM@EGDBE-E is dense and uniform, and there is an absence of intragranular crack throughout the particle (**Figure 6c** and **Figure S43c**). In addition, the particle is composed of uniform layered lattice fringes without any defective region or second phase (**Figure 6f** and **Figure S44e**). Last, the surface of these primary particles was characterized to study the phase transition and CEI. As shown in **Figure 6g-l**, compared with the pristine NCM811 particle (**Figure S46**), in all samples rock-salt layers ($Fm\bar{3}m$ phase) are formed due to the accumulation of Ni^{2+}/Li^{+} cation mixing during battery cycling,[7c] as verified by the fast Fourier transform (FFT) patterns in **Figure S47**, which is covered by amorphous CEI layers (**Figure 6j-l**). The thickness of the CEI layer is reduced from 6-7 nm in NCM@EGDME-E to 5-6 nm in

NCM@EGDEE-E, and 1.5 nm in NCM@EGDBE-E, which is consistent with the XPS results in **Figure 5a**. In addition, the thickness of the rock-salt layer has also been reduced from 4-5 nm in NCM@EGDME-E to 3-4 nm in NCM@EGDEE-E and 1.5 nm in NCM@EGDBE-E. Both the XPS and STEM results confirm that with the extension of terminal alkyl chains in ether solvents, the NCM811-electrolyte interactions have been suppressed and the interface has been stabilized, which significantly improved the structural stability and electrochemical performance of NCM811 cathode.

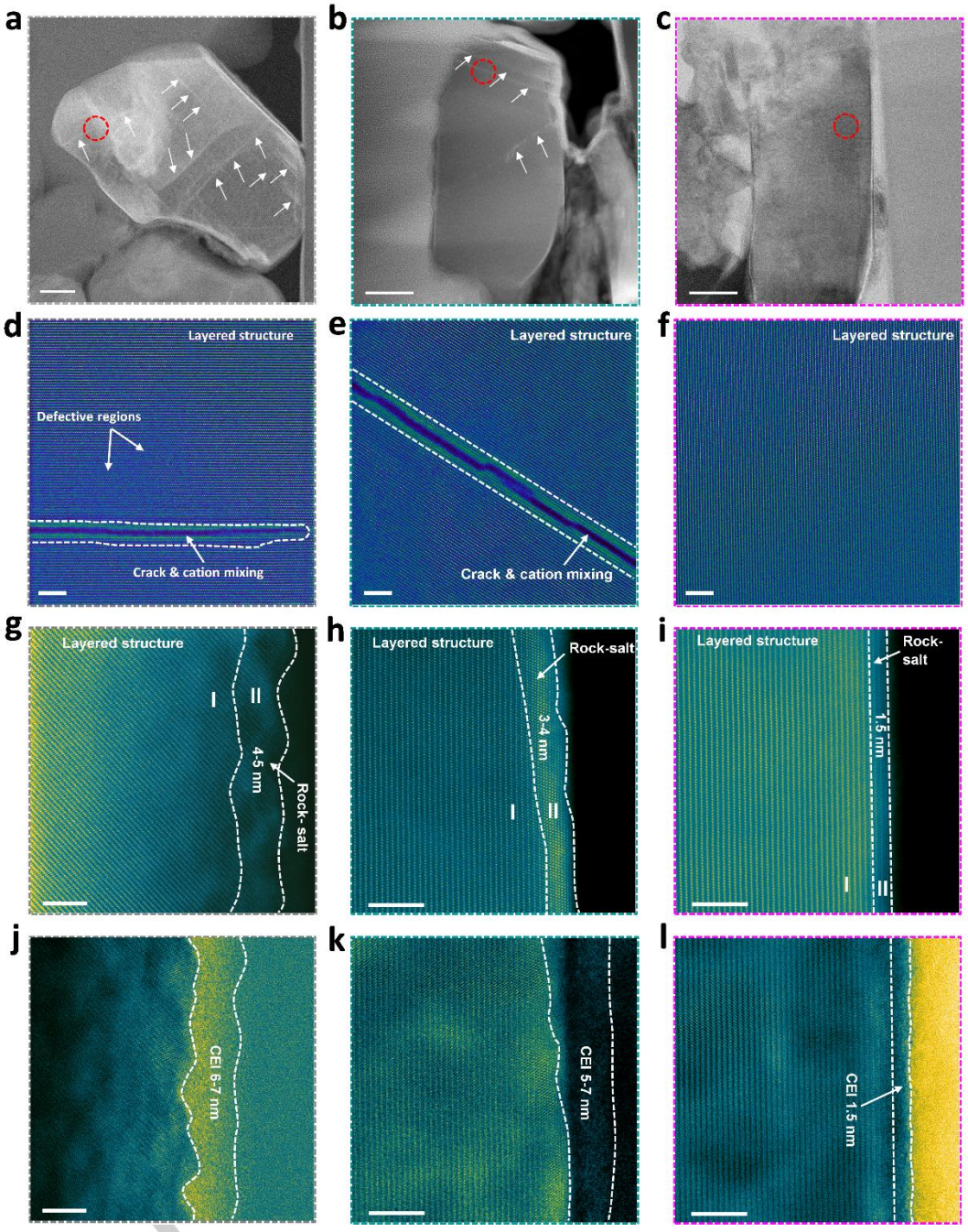

Figure 6. STEM imaging on NCM811 cathodes cycled in three electrolytes for 100 cycles at 60 ℃. (a-i) HAADF-STEM images of the secondary particles of NCM811 cycled in EGDME-E (a,d,g), EGDEE-E (b,e,h), and EGDBE-E (c,f,i), showing their overall morphology (a-c), inner (d-f) and surface (g-i) structure. The arrows in (a,b) indicate the intragranular cracks. The imaged area in (d-f) corresponds to the circled regions in (a-c). (j-l) ABF-STEM images of the surface area of NCM811 cycled in EGDME-E (j), EGDEE-E (k), and EGDBE-E (l). Scale bars, a-c: 100 nm; d-f: 10 nm; and g-l: 5 nm.

Conclusion

To conclude, we have shown that tuning the terminal alkyl chains in ethers can stabilize the electrode-electrolyte interfaces and prolong the lifespan of high-temperature NCM811-Li batteries. With the extension of terminal alkoxy groups to ethoxy groups and

n-butoxy groups in glycol diethers, the comprehensive stability of electrolytes against both Li metal anode and NCM811 cathode is improved, and an anion-dominated solvation structure is achieved. Consequently, the electrode-electrolyte interaction has been suppressed, a thinner, denser, and more inorganic-rich SEI/CEI has been constructed, and the structural dehydration of the NCM cathode is alleviated. The reversibility for Li plating/stripping has been boosted to 99.41% even at a high temperature of 60 °C. The cycling life of high-temperature NCM811-Li batteries has been boosted by more than 400% with a high CE of 99.77% at quasi-practical conditions. This work proved that beyond increasing salt concentration and using fluorinated solvents, extending terminal alkyl chains of ether solvents is a simple but effective strategy to regulate electrolyte solvation structure and stabilize electrode-electrolyte interfaces. This design principle can be extended to developing advanced electrolytes for other alkali metal/ion batteries.

Acknowledgements

This work was supported by the General Research Fund scheme of the Hong Kong Research Grants Council (15301220), the Hong Kong Polytechnic University (YXAU, CDBJ and ZVRP). The TEM facility is funded by the Research Grants Council of Hong Kong (Project No. C5029-18E).

Author contributions

Z. W. and B. Z. conceived the idea and designed the experiments. Z. W. conducted all electrochemical tests and analysed the data. D. W. and Z. W. conducted AFM test. C. C. performed FIB and TEM characterization under the supervision of Y. Z. Z. W. conducted other characterizations and wrote the manuscript with input from all the authors. B. Z. supervised the project.

Keywords: Ether electrolytes • alkoxy groups • terminal alkyl chains • high-temperature NCM811-Li batteries • electrode-electrolyte interfaces

References

[1] a) B. Liu, J.-G. Zhang and W. Xu, *Joule* **2018**, *2*, 833-845; b) D. Lin, Y. Liu and Y. Cui, *Nature Nanotechnology* **2017**, *12*, 194-206; c) Z. Wang, Y. Wang, B. Li, J. C. Bouwer, K. Davey, J. Lu and Z. Guo, *Angewandte Chemie International Edition* **2022**, *61*, e202206682.

[2] J. Liu, Z. Bao, Y. Cui, E. J. Dufek, J. B. Goodenough, P. Khalifah, Q. Li, B. Y. Liaw, P. Liu, A. Manthiram, Y. S. Meng, V. R. Subramanian, M. F. Toney, V. V. Viswanathan, M. S. Whittingham, J. Xiao, W. Xu, J. Yang, X.-Q. Yang and J.-G. Zhang, *Nature Energy* **2019**, *4*, 180-186.

[3] a) X. Yu and A. Manthiram, *Energy & Environmental Science* **2018**, *11*, 527-543; b) Y. Wu, X. Liu, L. Wang, X. Feng, D. Ren, Y. Li, X. Rui, Y. Wang, X. Han, G.-L. Xu, H. Wang, L. Lu, X. He, K. Amine and M. Ouyang, *Energy Storage Materials* **2021**, *37*, 77-86; c) H. Maleki Kheimeh Sari and X. Li, *Advanced Energy Materials* **2019**, *9*, 1901597.

[4] a) Y. Wang, Z. Wang, L. Zhao, Q. Fan, X. Zeng, S. Liu, W. K. Pang, Y.-B. He and Z. Guo, *Advanced Materials* **2021**, *33*, 2008133; b) Z. Wang, Y. Wang, Z. Zhang, X. Chen, W. Lie, Y.-B. He, Z. Zhou, G. Xia and Z. Guo, *Advanced Functional Materials* **2020**, *30*, 2002414; c) P. Zhai, L. Liu, X. Gu, T. Wang and Y. Gong, *Advanced Energy Materials* **2020**, *10*, 2001257.

[5] L. Suo, W. Xue, M. Gobet, S. G. Greenbaum, C. Wang, Y. Chen, W. Yang, Y. Li and J. Li, *Proceedings of the National Academy of Sciences* **2018**, *115*, 1156-1161.

[6] Y. Chen, Q. He, Y. Mo, W. Zhou, Y. Zhao, N. Piao, C. Liu, P. Xiao, H. Liu, B. Li, S. Chen, L. Wang, X. He, L. Xing and J. Liu, *Advanced Energy Materials* **2022**, *12*, 2201631.

[7] a) L. Zou, Z. Liu, W. Zhao, H. Jia, J. Zheng, Y. Yang, G. Wang, J.-G. Zhang and C. Wang, *Chemistry of Materials* **2018**, *30*, 7016-7026; b) C. Liang, F. Kong, R. C. Longo, S. Kc, J.-S. Kim, S. Jeon, S. Choi and K. Cho, *The Journal of Physical Chemistry C* **2016**, *120*, 6383-6393; c) W. Liu, P. Oh, X. Liu, M.-J. Lee, W. Cho, S. Chae, Y. Kim and J. Cho, *Angewandte Chemie International Edition* **2015**, *54*, 4440-4457.

[8] L. Wang, Q. Su, B. Han, W. Shi, G. Du, Y. Wang, H. Li, L. Gu, W. Zhao, S. Ding, M. Zhang, Y. Yang and B. Xu, *Journal of Energy Chemistry* **2023**, *77*, 428-437.

[9] D. Zhang, M. Liu, J. Ma, K. Yang, Z. Chen, K. Li, C. Zhang, Y. Wei, M. Zhou, P. Wang, Y. He, W. Lv, Q.-H. Yang, F. Kang and Y.-B. He, *Nature Communications* **2022**, *13*, 6966.

[10] a) Z. Wang, Y. Wang, C. Wu, W. K. Pang, J. Mao and Z. Guo, *Chemical Science* **2021**, *12*, 8945-8966; b) Q. Zhang, S. Liu, Y. Lu, L. Xing and W. Li, *Journal of Energy Chemistry* **2021**, *58*, 198-206; c) Y. Gao, Z. Yan, J. L. Gray, X. He, D. Wang, T. Chen, Q. Huang, Y. C. Li, H. Wang, S. H. Kim, T. E. Mallouk and D. Wang, *Nature Materials* **2019**, *18*, 384-389; d) N.-W. Li, Y.-X. Yin, C.-P. Yang and Y.-G. Guo, *Advanced Materials* **2016**, *28*, 1853-1858.

[11] J.-M. Kim, X. Zhang, J.-G. Zhang, A. Manthiram, Y. S. Meng and W. Xu, *Materials Today* **2021**, *46*, 155-182.

[12] H. Wang, Z. Yu, X. Kong, S. C. Kim, D. T. Boyle, J. Qin, Z. Bao and Y. Cui, *Joule* **2022**, *6*, 588-616.

[13] Y. Jie, X. Ren, R. Cao, W. Cai and S. Jiao, *Advanced Functional Materials* **2020**, *30*, 1910777.

[14] a) X. Ren, L. Zou, S. Jiao, D. Mei, M. H. Engelhard, Q. Li, H. Lee, C. Niu, B. D. Adams, C. Wang, J. Liu, J.-G. Zhang and W. Xu, *ACS Energy Letters* **2019**, *4*, 896-902; b) S. Jiao, X. Ren, R. Cao, M. H. Engelhard, Y. Liu, D. Hu, D. Mei, J. Zheng, W. Zhao, Q. Li, N. Liu, B. D. Adams, C. Ma, J. Liu, J.-G. Zhang and W. Xu, *Nature Energy* **2018**, *3*, 739-746.

[15] a) Z. Yu, H. Wang, X. Kong, W. Huang, Y. Tsao, D. G. Mackanic, K. Wang, X. Wang, W. Huang, S. Choudhury, Y. Zheng, C. V. Amanchukwu, S. T. Hung, Y. Ma, E. G. Lomeli, J. Qin, Y. Cui and Z. Bao, *Nature Energy* **2020**, *5*, 526-533; b) Y. Zhao, T. Zhou, M. Mensi, J. W. Choi and A. Coskun, *Nature Communications* **2023**, *14*, 299; c) Z. Yu, P. E. Rudnicki, Z. Zhang, Z. Huang, H. Celik, S. T. Oyakhire, Y. Chen, X. Kong, S. C. Kim, X. Xiao, H. Wang, Y. Zheng, G. A. Kamat, M. S. Kim, S. F. Bent, J. Qin, Y. Cui and Z. Bao, *Nature Energy* **2022**, *7*, 94-106; d) C. V. Amanchukwu, Z. Yu, X. Kong, J. Qin, Y. Cui, Z. N. Bao, *Journal of the American Chemical Society* **2020**, 142, 7393– 7403.

[16] a) Z. Li, H. Rao, R. Atwi, B. M. Sivakumar, B. Gwalani, S. Gray, K. S. Han, T. A. Everett, T. A. Ajantiwalay, V. Murugesan, N. N. Rajput and V. G. Pol, *Nature Communications* **2023**, *14*, 868; b) K. Ding, C. Xu, Z. Peng, X. Long, J. Shi, Z. Li, Y. Zhang, J. Lai, L. Chen, Y.-P. Cai and Q. Zheng, *ACS Applied Materials & Interfaces* **2022**, *14*, 44470-44478; c) Y. Chen, Z. Yu, P. Rudnicki, H. Gong, Z. Huang, S. C. Kim, J.-C. Lai, X. Kong, J. Qin, Y. Cui and Z. Bao, *Journal of the American Chemical Society* **2021**, *143*, 18703-18713; d) E. Park, J. Park, K. Lee, Y. Zhao, T. Zhou, G. Park, M.-G. Jeong, M. Choi, D.-J. Yoo, H.-G. Jung, A. Coskun and J. W. Choi, *ACS Energy Letters* **2023**, *8*, 179-188; e) J. Zhang, Q. Li, Y. Zeng, Z. Tang, D. Sun, D. Huang, Y. Tang, and H. Wang, *ACS Energy Letters* **2023**, 8, 4, 1752-1761; f) T. D. Pham, A. Bin Faheem, J. Kim, H. M. Oh, K.-K. Lee, *Small* **2022**, 18, 2107492.

[17] a) J. B. Goodenough and Y. Kim, *Chemistry of Materials* **2010**, *22*, 587-603; b) P. Peljo and H. H. Girault, *Energy & Environmental Science* **2018**, *11*, 2306-2309.

[18] a) W. Xue, R. Gao, Z. Shi, X. Xiao, W. Zhang, Y. Zhang, Y. G. Zhu, I. Waluyo, Y. Li, M. R. Hill, Z. Zhu, S. Li, O. Kuznetsov, Y. Zhang, W.-K. Lee, A. Hunt, A. Harutyunyan, Y. Shao-Horn, J. A. Johnson and J. Li, *Energy & Environmental Science* **2021**, *14*, 6030-6040; b) S.-J. Cho, D.-E. Yu, T.

P. Pollard, H. Moon, M. Jang, O. Borodin and S.-Y. Lee, *iScience* **2020**, *23*, 100844.

[19] a) W. Sun, T. Tao, R. Zhang, W. Li, J. Yang and B. Yang, *Combustion and Flame* **2018**, *191*, 298-308; b) L. E. Camacho-Forero and P. B. Balbuena, *Physical Chemistry Chemical Physics* **2017**, *19*, 30861-30873; c) J. Huang, X. Guo, X. Du, X. Lin, J.-Q. Huang, H. Tan, Y. Zhu and B. Zhang, *Energy & Environmental Science* **2019**, 12, 1550-1557.

[20] W. Wahyudi, V. Ladelta, L. Tsetseris, M. M. Alsabban, X. Guo, E. Yengel, H. Faber, B. Adilbekova, A. Seitkhan, A.-H. Emwas, M. N. Hedhili, L.-J. Li, V. Tung, N. Hadjichristidis, T. D. Anthopoulos and J. Ming, *Advanced Functional Materials* **2021**, *31*, 2101593.

[21] J. Wang, W. Huang, A. Pei, Y. Li, F. Shi, X. Yu and Y. Cui, *Nature Energy* **2019**, *4*, 664-670.

[22] C. Fang, J. Li, M. Zhang, Y. Zhang, F. Yang, J. Z. Lee, M.-H. Lee, J. Alvarado, M. A. Schroeder, Y. Yang, B. Lu, N. Williams, M. Ceja, L. Yang, M. Cai, J. Gu, K. Xu, X. Wang and Y. S. Meng, *Nature* **2019**, *572*, 511-515.

[23] a) X. Zhang, H. Jia, L. Zou, Y. Xu, L. Mu, Z. Yang, M. H. Engelhard, J.-M. Kim, J. Hu, B. E. Matthews, C. Niu, C. Wang, H. Xin, F. Lin, and Wu Xu, *ACS Energy Letters* **2021**, 6, 4, 1324-1332; b) Y. Lee, T. K. Lee, S. Kim, J. Lee, Y. Ahn, K. Kim, H. Ma, G. Park, S.-M. Lee, S. K. Kwak, and N.-S. Choi, *Nano Energy* **2020**, 67, 104309.

[24] R. A. Huggins in *Solid Electrolyte Battery Materials*, *Vol.* STANFORD UNIV CALIF CENTER FOR MATERIALS RESEARCH, **1977**.

[25] a) Y. Zhao, T. Zhou, L. P. H. Jeurgens, X. Kong, J. W. Choi and A. Coskun, *Chem* **2023**, 9, 682-697; b) H. Chen, A. Pei, D. Lin, J. Xie, A. Yang, J. Xu, K. Lin, J. Wang, H. Wang, F. Shi, D. Boyle and Y. Cui, *Advanced Energy Materials* **2019**, *9*, 1900858.

[26] X. Cao, X. Ren, L. Zou, M. H. Engelhard, W. Huang, H. Wang, B. E. Matthews, H. Lee, C. Niu, B. W. Arey, Y. Cui, C. Wang, J. Xiao, J. Liu, W. Xu and J.-G. Zhang, *Nature Energy* **2019**, *4*, 796-805.

Table of Contents

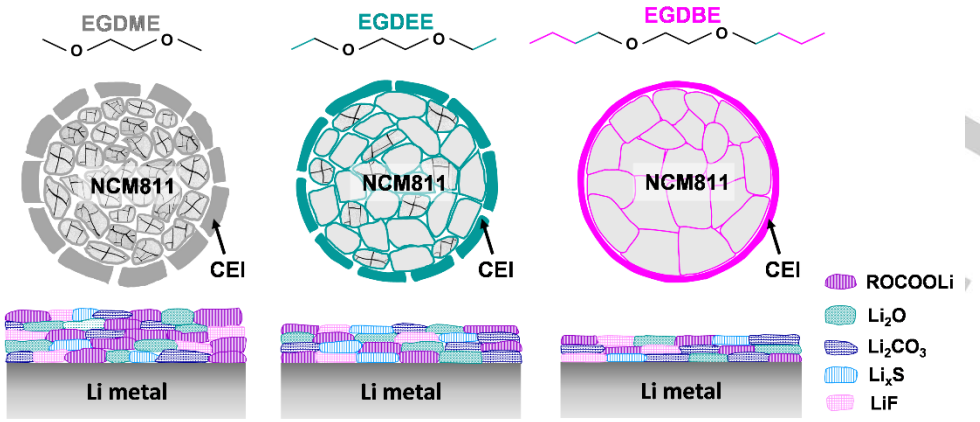

We propose that by extending the terminal groups of glycol diethers from methyl groups to *n*-butyl groups, the comprehensive stability of ether electrolytes can be improved. An anion-dominated solvation structure is realized at 1 M. The electrode-electrolyte interactions are suppressed, and a thinner, denser, and more inorganic-rich SEI/CEI is achieved. The phase transition and structural degradation of the NCM811 cathode are also alleviated.